American Mineralogist, Volume 95, pages 639–645, 2010

A new type of cubic-stacked layer structure in anthoinite, $AlWO_3(OH)_3$

Ian E. Grey,[1,*] Ian C. Madsen,[1] Stuart J. Mills,[2] Frederic Hatert,[3] Vanessa K. Peterson,[4] and Timothy J. Bastow[5]

[1]CSIRO Minerals, Box 312, Clayton South, Victoria 3169, Australia
[2]Department of Earth and Ocean Sciences, University of British Columbia, Vancouver, British Columbia V6T 1Z4, Canada
[3]Laboratoire de Minéralogie et de Cristallochimie, B-18, Université de Liège, B-4000 Liège, Belgium
[4]Bragg Institute, ANSTO, PMB 1, Menai, New South Wales 2234, Australia
[5]CSIRO Materials Science and Engineering, Private Bag 33, Clayton South, Victoria 3169, Australia

Abstract

Anthoinite, $AlWO_3(OH)_3$, from the Mt. Misobo Mine, Democratic Republic of the Congo, has triclinic symmetry with cell parameters $a = 8.196(1)$ Å, $b = 9.187(1)$ Å, $c = 11.316(1)$ Å, $\alpha = 92.82(1)°$, $\beta = 94.08(1)°$, $\gamma = 90.23(1)°$, space group $I\bar{1}$, $Z = 8$. The structure was solved by applying ab initio structure solution methods (Reverse Monte Carlo/Simulated Annealing) to both X-ray and neutron powder diffraction data and was refined using the Rietveld method. The structure is built up of two types of $M_4(O,OH)_{16}$ planar tetrameric clusters of edge-sharing octahedra, one containing predominantly Al and the other predominantly W. The Al-rich and W-rich clusters interconnect via corner sharing to form stepped layers parallel to (001). The layers are held together by strong hydrogen bonding. The structure can be described as a rocksalt derivative structure, with the close-packed anion layers parallel to (012), and with Al and W atoms ordered into one third of the octahedral sites within the cubic close-packed anion lattice. The structure is complicated by partial disorder between Al and W in the tetrameric clusters and associated disorder in the H atom sites. Infrared and ^{27}Al MAS NMR results are also presented for anthoinite.

Keywords: Structure of anthoinite, ab initio structure determination, new layer structure in $AlWO_3(OH)_3$, layer structure of anthoinite

Introduction

Varlamoff (1947) first described anthoinite from the Mt. Misobo tungsten mine, Democratic Republic of the Congo, where it forms microcrystalline masses, often pseudomorphed after scheelite. His chemical analyses conformed to the composition $Al_2O_3 \cdot 2WO_3 \cdot 3H_2O$. The first crystallographic studies on anthoinite were made by Niggli and Jager (1957). They reported the powder X-ray diffraction (XRD) pattern, and gave electron microscopy results, which showed that the crystals are generally submicrometer in size and have a platy habit. They determined the basal plane cell parameters from electron diffraction patterns of the oriented platelets ($a = 9.33$ Å, $b = 8.17$ Å) and proposed that the symmetry was monoclinic or triclinic. Sahama et al. (1970) studied samples of anthoinite from Uganda and Rwanda and confirmed the electron diffraction results of Niggli and Jager (1957). They used the preferred-orientation enhancement of basal plane reflections to determine the third crystal axis and indexed the powder pattern with a triclinic cell. From thermogravimetric analysis, they determined that the water was lost in the relatively high temperature range 400 to 545 °C, leading them to give the formula for anthoinite as $AlWO_3(OH)_3$. Sahama et al. (1970) commented that the pronounced cleavage exhibited by the mineral suggested a sheet structure. Sahama (1981) subsequently re-indexed the powder pattern and he gave the unit-cell dimensions of the new triclinic cell as $a = 9.21$ Å, $b = 11.36$ Å, $c = 8.26$ Å, $\alpha = 94.75°$, $\beta = 90.0°$, and $\gamma = 92.58°$.

* E-mail: ian.grey@csiro.au

The first occurrence of anthoinite outside Africa was reported by Matsubara et al. (1984). They identified anthoinite pseudomorphed after scheelite in the Kara tin/tungsten mine in northwest Tasmania. The anthoinite was intimately associated with mpororoite, $AlWO_3(OH)_3 \cdot nH_2O$, $n = 1–2$ (Von Knorring et al. 1972). Mpororoite has a powder pattern that is closely related to that for anthoinite, and it is considered to be a hydrated form of anthoinite.

It was not until 34 years after the discovery of anthoinite that consistent indexing of the powder pattern was obtained, and a further 28 years have lapsed without further reported advances on the crystal chemistry of the mineral. The low symmetry, relatively large cell volume, lack of single crystals, and combination of light (H, O) and heavy (W) atoms, all conspire to make the structure analysis difficult. In this study, we have used powder diffraction ab initio structure solution methods, applied to both X-ray and neutron diffraction data for anthoinite, to solve the structure. We report here the results of the structure analysis, together with thermal analyses, ^{27}Al MAS NMR, and infrared spectroscopy data for the mineral.

Experimental methods

A white, microcrystalline sample of anthoinite from the Mt. Misobo Mine, Kalima mining district, Maniema Province, Democratic Republic of the Congo, was used for the study. Chemical analyses of this material were reported by Varlamoff (1947). Thermogravimetric analyses (TGA) were conducted in the temperature range 24–1000 °C using a Setaram Simultaneous TGA/DTA instrument model 92. The evolved gases were analyzed using a Balzers Thermostar QS422 mass spectrometer (MS). The sample mass of ~50 mg was contained in a platinum crucible

and heated at a constant rate of 10° min^{-1} in flowing high purity nitrogen.

The infrared spectrum of anthoinite was recorded with a Nicolet NEXUS spectrometer, from 32 scans with a 1 cm^{-1} resolution, over the 400–4000 cm^{-1} region. The sample was prepared by intimately mixing 2 mg of sample with KBr to obtain a 150 mg homogeneous pellet, which was subsequently dried for a few hours at 120 °C. To prevent contamination by water, the measurements were performed under a dry air purge.

The ^{27}Al magic angle spinning (MAS) NMR spectra were taken on a Bruker Avance 400 spectrometer in a nominal field of 9.395 T, at a frequency around 104.26 MHz, in a probe with a 2.5 mm rotor. The spectra were obtained using a two pulse echo sequence with pulse separation synchronized with the rotation frequency, so that with a pulse separation of 35 μs a rotation frequency of 28.55 kHz (≈$[35\ \mu s]^{-1}$) was used. At this rotation frequency, the innermost spinning side bands were well separated from any spectral features. The two pulses of the echo sequence were of duration 1 μs and the pulse sequence repetition time in file acquisition was between 1 and 5 s. The reference zero ^{27}Al shift was that of the $Al(H_2O)_6^{3+}$ ion, set using a dilute aqueous solution of $AlCl_3$.

Powder X-ray data on a pressed disk of anthoinite powder were collected using a Philips diffractometer, equipped with a graphite monochromator and employing Co*K*α radiation. The X-ray tube was operated at 40 kV and 40 mA with 1° divergent and scatter slits, a 0.3 mm receiving slit, and soller slits. Step scan intensity data were collected in the 2θ range 5 to 140°, using a step size of 0.02° and a step counting time of 9 s.

Neutron powder diffraction data were collected on Echidna, the high-resolution powder diffractometer at the Open Pool Australian Light water reactor (OPAL) facility at the Australian Nuclear Science and Technology Organisation (Liss et al. 2006). A 6 g sample of anthoinite was packed in a 9 mm diameter vanadium can and room-temperature data were acquired over 14 h in the 2θ range 5.5 to 164°, using a wavelength of 1.622 Å and a step interval of 0.025°. A data set was also collected on corundum (NIST SRM 676 standard) for wavelength calibration. The obtained neutron diffraction pattern for anthoinite has a very high background due to the large incoherent scattering contribution from hydrogen. Attempts were made to deuterate the sample to obtain a lower background, but the protons were not labile enough to exchange with the D_2O solution. A constant value was removed from each point in the pattern to lower the background to a few hundred counts at the lowest point.

Crystallographic software used in the structure analysis includes WinGX (Farrugia 1999) for direct and Patterson search methods of structure solution, TOPAS (Coelho 2007) for Le Bail pattern decomposition and Reverse Monte Carlo/Simulated Annealing structure determination strategy, and Fullprof (Rodriguez-Carvajal 1990) for Rietveld refinements. A CIF is deposited.[1]

Structure determination and refinement

A Le Bail decomposition (Le Bail et al. 1988) of the X-ray powder diffraction pattern was conducted using the triclinic cell parameters reported by Sahama (1981). A separate Le Bail fitting of the pattern without a unit cell and use of the generated reflection positions in an automated indexing routine (Coelho 2003) gave a triclinic cell with half the volume of the Sahama cell, a = 8.208 Å, b = 8.025 Å, c = 8.351 Å, α = 111.61°, β = 116.63°, γ = 62.43°, V = 426.8 $Å^3$. The Sahama cell can be generated from this cell using the transformation matrix (100, 011, $\bar{1}1\bar{1}$). The relationships between the unit-cell parameters of our cell and those of Sahama show that the Sahama cell is *I*-centered. As the Sahama cell is closer to orthogonal geometry, making the structural topology easier to visualize in relation to the cell, it was used for the structure analysis. The order of the cell parameters was changed to $a < b < c$ so that they match the reported cell parameters for the structurally related mineral mpororoite (Von Knorring et al. 1972). The reported experimental density for anthoinite of 4.78 g/cm^3 (Frisch 1975) is consistent with 8 formula units of $AlWO_3(OH)_3$ in the *I*-centered cell.

Application, through WinGX, of direct methods and a Patterson search method to the reflection list of intensities in the *I*-centered cell failed to give a structural model that could be refined. At least part of the reason for failure is the high degree of peak overlap in the triclinic cell, making intensity assignments problematic. A useful piece of information was gleaned, however, from the Patterson map, which helped in the subsequent analysis. The strongest peak in the map was considerably lower in intensity (relative to the origin peak) than the value calculated for a W-W vector between independent W atoms. This observation was common to maps calculated at different *d*-spacing resolutions, and suggested that the W and Al atoms are at least partially disordered over the metal atom sites.

A successful starting structural model for anthoinite in the centrosymmetric space group $I\bar{1}$ was obtained by applying a Reverse Monte Carlo approach with Simulated Annealing (SA) as implemented in TOPAS (Coelho 2007). Four independent metal atoms, 12 O atoms and 6 H atoms were distributed randomly in the cell as the starting configuration. Each of the metal atom sites had equal occupancy of W and Al. To prevent the model moving to physically unrealistic configurations, anti-bump constraints were used, limiting the closest approach of O atoms to 2.25 Å and of metal and O atoms to 1.55 Å. The pattern fitting was applied simultaneously to both the neutron and the X-ray diffraction data. The temperature regime macro AUTO(T), as implemented in TOPAS, with T = 5 was used. The profile parameters were transferred from the Le Bail fitting and then fixed for the SA. They included profile parameters using the Thomson-Cox-Hastings pseudo-Voigt profile function for both patterns. The procedure was run for 20 000 cycles, resulting in a reasonable fit to both diffraction patterns (Global R_{wp} = 0.13) and a sensible structure topology comprising tetrameric clusters of edge-sharing octahedra that were further connected into layers by corner-sharing of octahedra. Some of the octahedra, however, had unreasonably large distortions, and the O-H distances were not sensible.

In the next step, the metal atom positions were improved by Rietveld refinement using the X-ray diffraction data. The resulting model was then used in Rietveld refinement of the O atom positions using the neutron diffraction data. In these refinements, the original H atoms were removed and the protons were then located in difference Fourier maps. Cycling between the X-ray and neutron data refinements led to further improvements in the fits to the profiles. The X-ray data refinements included refinement of the Al/W occupancy of the metal atom sites. The final coordinates and site occupancies, together with refinement agreement indices are given in Table 1. Observed and calculated profiles for the Rietveld refinements of X-ray and neutron data are shown in Figures 1 and 2, respectively.

Results and discussion

The differential thermal analysis curve for anthoinite heated in nitrogen has a broad endotherm centered at 98 °C, due to water loss, and a relatively sharp endotherm centered at 422 °C, corresponding to loss of hydroxyls. The weight loss up to 220 °C is only 0.29 wt%, whereas the weight loss between 220 and 575 °C is 8.54%. For comparison the calculated weight loss for

Table 1. Rietveld refinement results for anthoinite

Atom	*x*	*y*	*z*	*B* (Å^2)	Site occupancy
M1	0.759(1)	0.4972(9)	0.8687(7)	2.19(9)	0.685(7)Al+0.315(7)W
M2	0.0477(6)	0.2475(6)	0.7542(5)	2.19(9)	0.70(1)W+0.30(1) Al
M3	0.450(2)	0.254(2)	0.233(1)	2.19(9)	0.875(5)Al+0.125(5)W
M4	0.2408(6)	0.5139(5)	0.6304(4)	2.19(9)	0.78(1)W+0.22(1)Al
O1*	0.751(2)	0.625(1)	0.707(2)	2.02(5)	1.0
O2*	0.222(2)	0.107(2)	0.708(2)	2.02(5)	1.0
O3*	0.897(2)	0.827(2)	0.590(1)	2.02(5)	1.0
O4*	0.432(2)	0.173(1)	0.900(1)	2.02(5)	1.0
O5	0.571(2)	0.104(1)	0.188(1)	2.02(5)	1.0
O6	0.420(2)	0.626(1)	0.688(1)	2.02(5)	1.0
O7	0.417(2)	0.614(1)	0.200(1)	2.02(5)	1.0
O8	0.415(1)	0.886(2)	0.323(1)	2.02(5)	1.0
O9	0.391(1)	0.355(1)	0.610(1)	2.02(5)	1.0
O10*	0.419(2)	0.167(2)	0.405(1)	2.02(5)	1.0
O11*	0.305(1)	0.964(1)	0.535(1)	2.02(5)	1.0
O12*	0.743(2)	0.407(2)	0.517(1)	2.02(5)	1.0
H1	0.205(2)	0.055(2)	0.649(1)	0.95(9)	0.74(3)
H2A	0.424(3)	0.266(3)	0.030(2)	0.95(9)	0.67(3)
H2B	0.415(4)	0.345(4)	0.018(3)	0.95(9)	0.33(3)
H3	0.239(2)	0.059(2)	0.164(1)	0.95(9)	1.0
H4	0.996(2)	0.417(2)	0.597(2)	0.95(9)	1.0
H5A	0.297(4)	0.909(4)	0.086(3)	0.95(9)	0.53(3)
H5B	0.295(4)	0.992(4)	0.054(3)	0.95(9)	0.47(4)
H5C	0.228(3)	0.786(3)	0.002(3)	0.95(9)	0.53(3)
H6	0.099(2)	0.285(2)	0.027(2)	0.95(9)	0.63(3)
H7	0.900(4)	0.419(3)	0.007(4)	0.95(9)	0.50(4)

Notes: $AlWO_3(OH)_3$; space group $I\bar{1}$. Z = 8. Cell: a = 8.196(1) Å, b = 9.187(1) Å, c = 11.316(1) Å, α = 92.82(1)°, β = 94.08(1)°, γ = 90.23(1)°. ND refinement: R_{wp} = 5.0, R_B = 4.9. XRD refinement: R_{wp} = 13.7, R_B = 6.8.
* These anions are protonated.

[1] Deposit item AM-10-020, CIF. Deposit items are available two ways: For a paper copy contact the Business Office of the Mineralogical Society of America (see inside front cover of recent issue) for price information. For an electronic copy visit the MSA web site at http://www.minsocam.org, go to the *American Mineralogist* Contents, find the table of contents for the specific volume/issue wanted, and then click on the deposit link there.

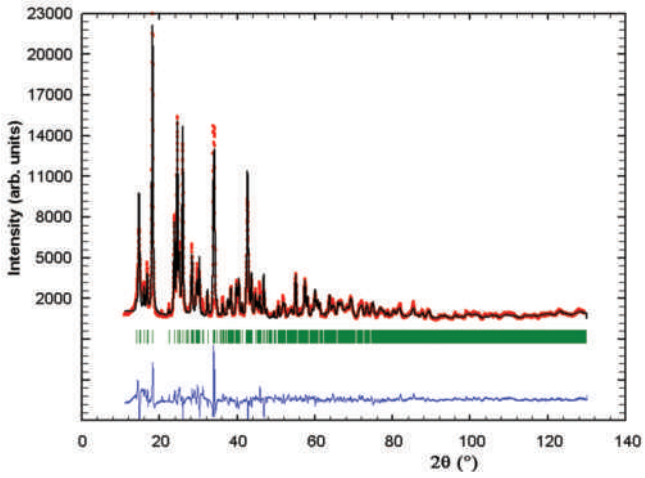

FIGURE 1. Rietveld fit (solid line) to experimental XRD pattern (circles) for anthoinite. The positions of the Bragg reflections and the difference plot are shown below the diffractograms.

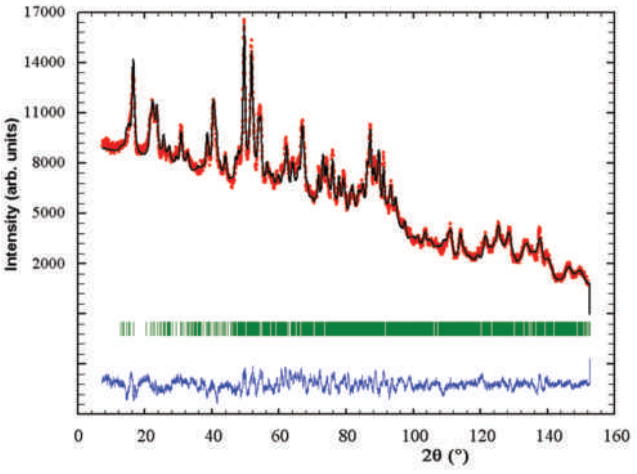

FIGURE 2. Rietveld fit (solid line) to experimental neutron diffraction pattern (circles) for anthoinite. The positions of the Bragg reflections and the difference plot are shown below the diffractograms.

$AlWO_3(OH)_3$ is 8.7%. Over 90% of the weight loss occurs in the interval 350 to 500 °C. The temperature range for the loss of hydroxyls is somewhat lower than the range of 400 to 545 °C reported by Sahama et al. (1970) and by Niggli and Jager (1957), who gave an endotherm minimum of 515 °C. A strong sharp exotherm occurs at 654 °C and a weaker exotherm at 854 °C, consistent with the DTA curve for anthoinite presented by Niggli and Jager (1957). The XRD pattern for a sample heated above the first exotherm, at 750 °C for 2 h, showed that the anthoinite had decomposed and was replaced by peaks due to $Al_2(WO_4)_3$ (PDF Card 11-5420).

A polyhedral representation of the structure of anthoinite is shown in projection down *c* in Figure 3. This shows that the structure-building motif is a tetrameric cluster of four edge-sharing octahedra. Each cluster shares eight octahedral vertices in pairs with four adjacent clusters to establish stepped layers parallel to (001). Each cluster has also two unshared octahedral vertices. There are two types of tetramers: those based on metal atoms M1 and M3 are Al-rich, while those comprising metal atoms M2

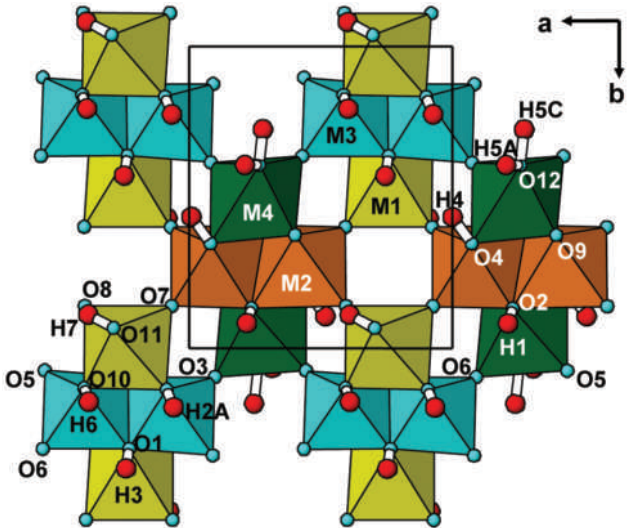

FIGURE 3. Polyhedral representation of the anthoinite structure projected along the *c* axis. Atom labels correspond to atoms in Table 1.

and M4 are W-rich, as shown by the site occupancies in Table 1. It is possible that full ordering occurs of Al and W in alternate tetramers within each layer, giving $Al_4(O,OH)_{16}$ and $W_4(O,OH)_{16}$ clusters, and that the apparent mixing of Al and W is due to layer stacking faults, as will be discussed in more detail below.

Calculated bond valence sums at the M and O sites, based on the bond valence parameters of Brese and O'Keeffe (1991) are given in Table 2. The calculated bond valences for the metal atom sites agree quite well with the expected valencies based on the Al^{3+} and W^{6+} contributions to each site (also given in Table 2), giving confidence in the site occupancies obtained from the structure refinement. As seen from Table 2, the mean difference is <0.2 valence units. The bond valence sums for the anion sites show clearly that the O5 to O9 sites are occupied by oxygen ions, while O1 to O4, O10, O11, and O12 are all severely undersaturated with valence sums in the range 0.63 to 1.38. Consistent with these calculations, the refinement confirmed that the protons are confined to the latter seven sites. The refinement using the neutron data showed that there is considerable disorder in the H atoms, with split (H2A/H2B and H5A/H5B/H5C) and partially occupied sites. This disorder is a reflection of the Al/W disorder in the metal atom sites. The sum of protons per asymmetric formula unit obtained from the site occupancy refinements, 6.4, is higher than expected for stoichiometric $Al_2W_2O_6(OH)_6$, but the difference is less than 2σ.

A representation of the structure of anthoinite projected approximately along [110] in Figure 4 shows the layer nature of the structure. There is no connectivity of the octahedra between adjacent (001) layers, which are held together by hydrogen bonding. The main interlayer hydrogen bonds are shown in Figure 4 and the hydrogen bond distances are given in Table 3. The bond O3-H2A···O4 is particularly strong, with H2A···O4 = 1.67 Å and O3-O4 = 2.55 Å. The bond O2-H1···O11 is also strong, with H1···O11 = 1.76 Å and O2-O11 = 2.44 Å. The anion O11 is the acceptor atom in this case and is also the donor atom in the bond O11-H7···O10. It might be expected that O2 is an

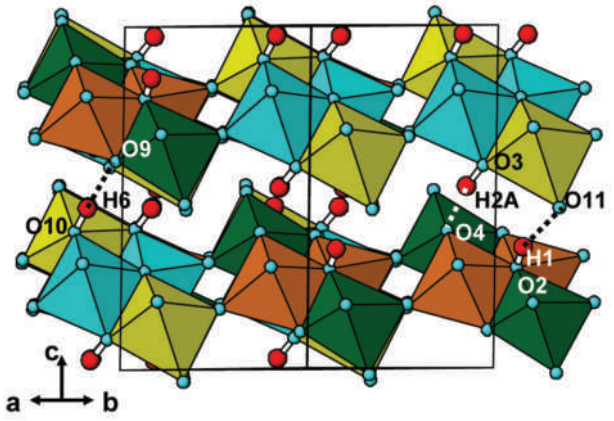

FIGURE 4. Projection of the structure of anthoinite along [110]. Interlayer H bonds shown.

unlikely site for a strong H-bond because it coordinates to three high-valency cations. However, as shown in Table 3, all of the O2-M distances are quite long, 2.01 to 2.31 Å, thus reducing the valence contributions of these metal atoms.

The infrared spectrum, shown in Figure 5, displays several peaks within the O-H stretching region that can be assigned to hydroxyls. They fall into two wavenumber ranges, 1900–2100 and 3000–3500 cm^{-1}, corresponding to strong and weak-to-medium strength hydrogen bonds, respectively (Libowitzky 1999). Application of Libowitzky's plots of IR wavenumbers vs. H···O and O-O suggests that that the two peaks at 1949 and 2076 cm^{-1} can be assigned to the strong hydrogen bonds mentioned above, O3-H2A···O4 and O2-H1···O11. The peak at 1646 cm^{-1} is located in the region for the H-O-H bending mode of water and may be associated with H_2O at the O12 site. As seen from Figure 3 and Table 3, H5A-O12-H5C has the correct geometry for a water molecule, within the relatively large errors associated with the disordered hydrogen positions.

A view of the anthoinite structure along [100] in Figure 6 reveals that it approximates a close-packed structure, with the close-packed anion layers parallel to (012). The layers are stacked according to the cubic stacking sequence ABC... The tetrameric metal-centered clusters are completely isolated from one another within the close-packed layers, and share corners with one another between adjacent layers. The repeat distance for six layers along [011] is 14.23 Å, giving a separation between the close-packed layers of 2.37 Å. It is important to emphasize the difference between the close-packed layer orientation, (012), shown in Figure 6 and the mean orientation of the stepped layers, (001), shown in Figure 4.

Planar tetrameric clusters of edge-shared octahedra containing Al have been recently reported in the compound $[Al_8(OH)_{14}(H_2O)_{18}](SO_4)_5 \cdot 16H_2O$ (Casey et al. 2005), while W-centered tetrameric clusters occur in the silver tungstate $Ag_8W_4O_{16}$ (Skarstad and Geller 1975). To the best of our knowledge, there are no known compounds in which the tetrameric clusters contain both trivalent and hexavalent cations. In anthoinite, it is possible that the Al^{3+} and W^{6+} cations are fully ordered into the sites M1, M3 and M2, M4, respectively, within each stepped (001) layer, and that the observed mixed occupancy of these sites is due to relative displacements of adjacent layers

TABLE 3. Selected bond lengths (Å) for anthoinite

M1-O8	1.73(2)	H1-O2	0.81(2)
M1-O7	1.86(2)	H1···O11	1.76(2)
M1-O11	1.93(1)	O2-O11	2.44(2)
M1-O10	2.04(2)		
M1-O3	2.12(2)	H2A-O3	0.90(3)
M1-O1	2.22(2)	H2A···O4	1.67(3)
Mean	1.98(1)	O3-O4	2.55(2)
		H2B-O3	0.86(4)
		H2A-H2B	0.75(5)
M2-O7	1.69(1)	H3-O1	0.76(2)
M2-O8	1.86(1)	H3···O12	2.12(2)
M2-O9	1.88(1)	O1-O12	2.86(2)
M2-O4	1.94(1)		
M2-O2	2.01(2)	H4-O4	1.02(2)
M2-O2	2.31(2)	H4···O5	2.03(2)
Mean	1.95(1)	O4-O5	2.69(1)
M3-O6	1.71(2)	H5A-O12	0.87(3)
M3-O5	1.78(2)	H5B-O12	0.95(4)
M3-O3	1.81(2)	H5C-O12	1.12(3)
M3-O1	2.01(2)	H5A-H5C	1.52(4)
M3-O1	2.12(2)		
M3-O10	2.17(2)	H6-O10	0.89(3)
Mean	1.93(1)	H6···O9	1.97(2)
		O9-O10	2.85(2)
M4-O5	1.77(2)	H7-O11	0.95(4)
M4-O6	1.85(2)	H7···O10	1.92(4)
M4-O12	1.87(1)	O10-O11	2.63(2)
M4-O9	1.93(1)		
M4-O2	2.19(2)		
M4-O4	2.22(1)		
Mean	1.97(1)		

TABLE 2. Bond valence sums (in valence units) for anthoinite (bond valence parameters from Brese and O'Keeffe 1991)

	M1 0.685 Al+0.315 W	M2 0.3 Al+0.7 W	M3 0.87 Al+0.13 W	M4 0.22 Al+0.78 W	Σv for O
O1	0.29		0.31, 0.43		1.03
O2		0.66, 0.29		0.43	1.38
O3	0.38		0.74		1.12
O4		0.80		0.40	1.20
O5			0.80	1.33	2.13
O6			0.97	1.07	2.04
O7	0.77	1.58			2.35
O8	1.09	0.99			2.08
O9		0.94		0.86	1.80
O10	0.57		0.28		0.85
O11	0.63				0.63
O12				1.02	1.02
Σv for M	3.73	5.26	3.53	5.11	
*From Al^{3+}/W^{6+}	3.94	5.10	3.39	5.34	

* 3 × SOF(Al) + 6 × SOF(W), where the SOFs are given at the top of the table.

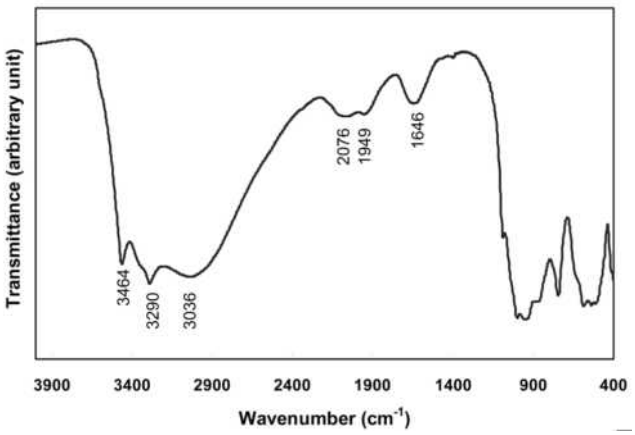

FIGURE 5. Infrared spectrum of anthoinite.

(stacking faults). An inspection of Figure 4 shows that tetramers containing M1/M3 lie directly above tetramers containing M2/M4 and vice versa in adjacent layers. A displacement of one layer relative to an adjacent layer by ½[110] results in an unchanged topology but with interchanged M1/M3 and M2/M4 tetramers, so that at the stacking fault, like-tetramers are aligned vertically.

Direct verification of such stacking faults by transmission electron microscopy would be difficult, given the pronounced (001) cleavage of the micrometer-sized platelet crystals. Previous TEM studies have succeeded in obtaining only the a^*b^* reciprocal lattice section (Niggli and Jager 1957; Sahama et al. 1970). We have seen some evidence of faulting in the powder X-ray diffraction patterns for different samples of anthoinite, where the intensity and halfwidth of the (011) peak (first observable peak in the XRD pattern in Fig. 1) both vary considerably between samples. Structure factor calculations show that the intensity of this reflection is particularly sensitive to the extent of Al/W ordering.

Indirect evidence for ordering of Al in one tetramer and W in the other comes from the ^{27}Al MAS NMR spectrum, shown in Figure 7. It displays a single, nearly symmetric resonance with a chemical shift of +1.5 ppm. The peak is relatively broad, with a halfwidth of 13 ppm. The broadening is likely due to second-order nuclear quadrupole interaction (NQI), since the AlO_6 octahedra are considerably distorted. There may be a smaller contribution to the broadening from a near superposition of peaks from the Al atoms in the four independent sites, M1 to M4. The slight asymmetry of the lineshape (distribution of NQI parameters) indicates some degree of disorder, consistent with the structure refinement.

Multi-quantum (MQ) MAS NMR experiments have been reported on related structures. MQMAS removes all the nuclear quadrupole interaction while MAS alone only removes part of this interaction. MQMAS NMR measurements on $[Al_8(OH)_{14}(H_2O)_{18}](SO_4)_5 \cdot 16H_2O$ reveal that the two independent Al sites in the $Al_4(OH)_{14}(H_2O)_2$ tetramers have chemical shifts of 8.4 and 11.0 ppm (Casey et al. 2005). The smaller ^{27}Al chemical shift in anthoinite may reflect the influence of adjacent corner-connected WO_6 octahedra. For comparison, in $Al_2(MoO_4)_3$, where individual AlO_6 octahedra are completely surrounded by six corner-connected MoO_4 tetrahedra, the ^{27}Al MAS NMR peaks are much more strongly shifted, to negative values in the range

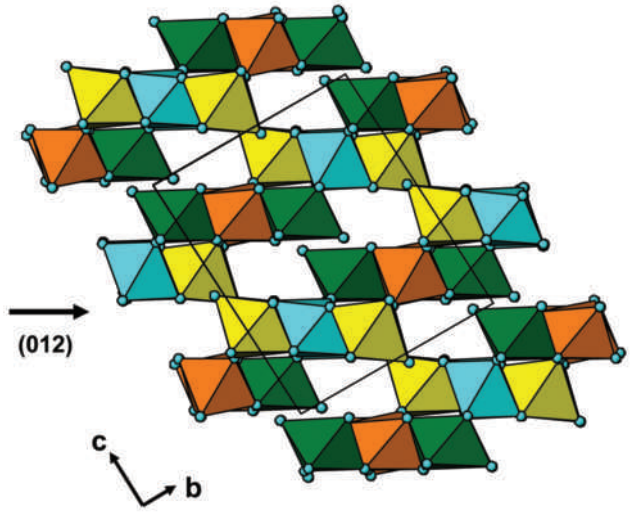

FIGURE 6. Projection of the anthoinite structure along [100]. The orientation of the close-packed (012) layers is indicated by the arrow. The H atoms are omitted for clarity.

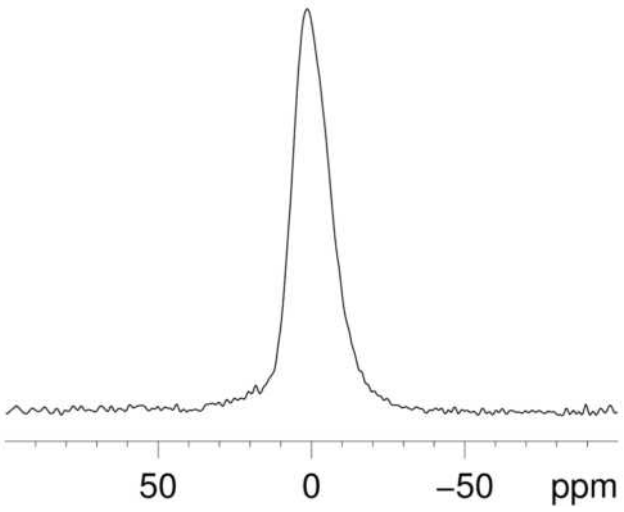

FIGURE 7. The ^{27}Al MAS NMR spectrum for anthoinite.

–9.5 to –12.1 ppm (Haddix et al. 1993).

The anthoinite structure can be considered as a rocksalt-derivative structure in which only one third of the metal atom sites in a cubic close-packed anion lattice are occupied in an ordered pattern. In such situations, where high valency cations occupy a minor fraction of sites in a close-packed lattice of anions, the lowest energy structure is often achieved by forming a layer structure. In this context, a related mineral is molybdite, MoO_3, which has the same stoichiometry and same anion cubic close-packing as in anthoinite. Molybdite has orthorhombic symmetry, *Pbnm*, with $a = 3.963$ Å, $b = 13.855$ Å, $c = 3.696$ Å (Kihlborg 1963). The stepped layers of occupied octahedra are parallel to (010), whereas the close-packed layers are parallel to $(13\bar{1})$. In molybdite, isolated pairs of edge-shared octahedra occur within the close-packed layers. The octahedra in adjacent layers share edges and corners, building up anatase-like, stepped, double layers of octahedra. The octahedra in molybdite show the same

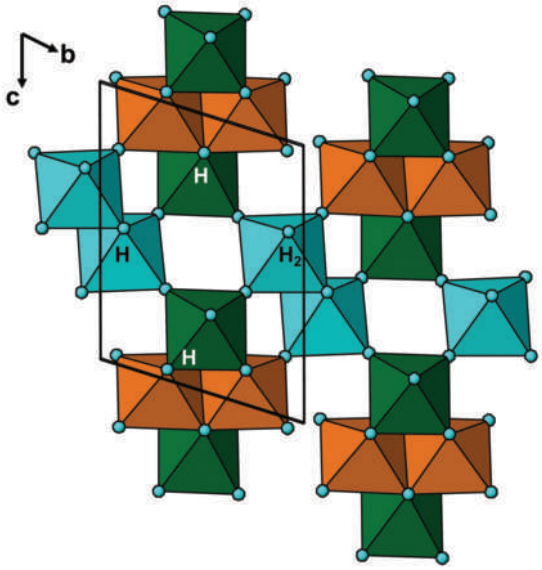

FIGURE 8. The layer structure of bamfordite (Birch et al. 1998) viewed in projection normal to the layers; compare with the same projection of anthoinite in Figure 3.

wide range of bond lengths (1.67 to 2.33 Å) as in anthoinite.

A search of the literature for structures related to that of anthoinite located the interesting example of the mineral bamfordite, $Fe^{3+}Mo_2O_6(OH)_3 \cdot H_2O$ (Birch et al. 1998) with a similar layer structure. A projection of the bamfordite structure along the normal to the layers is shown in Figure 8, where it can be compared with anthoinite in the equivalent projection in Figure 3. Both structures have planar tetrameric clusters containing hexavalent cations that form layers by sharing peripheral anions with adjacent clusters containing trivalent cations. Whereas in anthoinite the adjacent clusters are also tetrameric units, $Al_4^{3+}(O,OH)_{16}$, in bamfordite the tetramers interconnect with octahedral dimers $Fe_2^{3+}(O,OH,H_2O)_{10}$. Birch et al. (1998) noted a systematic trend in Mo-O distances within the $Mo_4(O,OH)_{16}$ tetramers, with average Mo-O distances decreasing from 2.25 to 1.94 to 1.69 Å for bonds involving μ3-O, μ2-O, and μ1-O, respectively (μn-O indicates bonding of the oxygen to n cations). A similar trend is observed for anthoinite, but with a smaller range of average distances, 2.14 to 2.01 to 1.90 Å.

Birch et al. (1998) did not determine the positions of the H atoms in bamfordite, but they used the results of bond valence calculations to suggest which anions were OH and H_2O. These are marked on Figure 8. There are similarities between the proton positions in the two structures. The protons are confined to the intra-cluster anions in both cases, with oxygen occupying all inter-cluster shared anion sites. The asymmetric occupation of only one of the two intracluster μ2-O sites in the $M_4^{6+}(O,OH)_{16}$ clusters is also common to both structures, as is the protonation of the μ3-O anions.

RELATIONSHIP OF MPORORITE TO ANTHOINITE

Mpororoite is the hydrated form of $AlWO_3(OH)_3$, first described by Von Knorring et al. (1972). The sample they studied, from the Mpororo tungsten mine in Uganda, contained similar amounts of Al_2O_3 and Fe_2O_3 and about twice the water content of anthoinite. The formula was expressed as $(Al,Fe)_2O_3 \cdot 2WO_3 \cdot 6H_2O$. Their thermal analysis studies showed that a similar amount (~8%) of water was lost above 200 °C as for anthoinite, so that the formula can be written as $(Al,Fe)WO_3(OH)_3 \cdot 1.5H_2O$. Matsubara et al. (1984) found mpororoite coexisting with anthoinite at the Kara tin/tungsten mine in Tasmania. Their material contained only 1.3 wt% Fe_2O_3, in contrast to the 9.9 wt% Fe_2O_3 in the Ugandan sample. Matsubara et al. (1984) were able to convert mpororoite to anthoinite by heating at 100 °C and then to reverse the transformation by soaking in water, thus indicating a close structural relationship between the two.

Von Knorring et al. (1972) indexed the powder pattern of mpororoite using a monoclinic cell with parameters $a = 8.27$ Å, $b = 9.32$ Å, $c = 16.40$ Å, and $\beta = 92.5°$. The a and b parameters for mpororoite are the same as those for anthoinite, suggesting that the structure is made up of the same type of layers, shown in Figure 3, with water molecules packed between the layers and expanding the interlayer spacing from 5.6 Å (=0.5 c) to 8.2 Å. Sahama (1981) subsequently re-evaluated the unit-cell data for mpororoite using 2-D electron diffraction patterns for the mineral. He obtained a cell close to that for anthoinite. When his parameters are re-ordered as for our anthoinite cell they are $a = 8.26$ Å, $b = 9.40$ Å, $c = 11.46$ Å, $\alpha = 94.3°$, $\beta = 95.2°$, and $\gamma = 89.7°$. The volume of this cell, 877 Å^3, is only 2.7% greater than that for anthoinite. It is possible that the water molecules can be accommodated in the layer structure without significant volume increase by a rearrangement of the anions toward denser packing, since the volume per anion in anthoinite is relatively high at 17.8 Å^3 (cf. a volume per anion of 14.7 in the close-packed structure of $AlWO_4$; Doumerc et al. 1975). The strongest peak in the mpororoite powder XRD pattern indexes as (100) in the triclinic cell. This reflection is forbidden in the diffraction pattern of the I-centered anthoinite, so that a different disposition of the layers relative to one another is required in mpororoite if the triclinic cell is correct. A density determination on a clean sample of mpororoite would distinguish between models based on the original, low-density monoclinic cell and Sahama's proposed triclinic cell. Despite having a structural model for anthoinite, the determination of the mpororoite structure from powder data still presents a significant challenge.

ACKNOWLEDGMENTS

We thank Nicki Agron-Olshina for collecting the X-ray diffraction data. Thanks to Graham Sparrow and to Nick Wilson from CSIRO Minerals for their reviews and helpful comments. F.H. thanks the FRS-F.N.R.S. (Belgium) for a position of "Chercheur qualifié."

REFERENCES CITED

Birch, W.D., Pring, A., McBriar, E.M., Gatehouse, B.M., and McCammon, C.A. (1998) Bamfordite, $Fe^{3+}Mo_2O_6(OH)_3 \cdot H_2O$, a new hydrated iron molybdenum oxyhydroxide from Queensland, Australia: Description and crystal chemistry. American Mineralogist, 83, 172–177.

Brese, N.E. and O'Keeffe, M. (1991) Bond-valence parameters for solids. Acta Crystallographica, B47, 192–197.

Casey, W.H., Olmstead, M.M., and Phillips, B.L. (2005) A new aluminum hydroxide octamer, $[Al_8(OH)_{14}(H_2O)_{18}](SO_4)_5 \cdot 16H_2O$. Inorganic Chemistry, 44, 4888–4890.

Coelho, A.A. (2003) Indexing of powder patterns by iterative use of singular value decomposition. Journal of Applied Crystallography, 36, 86–95.

——— (2007) TOPAS 4.1 Technical manual. Bruker AXS, Madison, Wisconsin.

Doumerc, J.P., Vlasse, M., Pouchard, M., and Hagenmuller, P. (1975) Synthèse, croissance cristalline, propriétés structurales et physiques d'un nouveau

tungstate +V d'aluminium $AlWO_4$. Journal of Solid State Chemistry, 14, 144–151.
Farrugia, L.J. (1999) WinGX suite for small-molecule single-crystal crystallography. Journal of Applied Crystallography, 32, 837–838.
Frisch, W. (1975) Die Wolfram-Lagerstatte Gifurwe (Rwanda) und die Genese der zentralafrikanischen Reinit-Lagerstatten. Jahrbuch der Geologischen Bundesanstalt, Wien, 118, 119–191.
Haddix, G.W., Narayana, M., Tang, S.C., and Wu, Y. (1993) Double-rotation NMR, magic angle spinning NMR and X-ray diffraction study of the structure of aluminum molybdate. Journal of Physical Chemistry, 97, 4624–4627.
Kihlborg, L. (1963) Least squares refinement of the structure of molybdenum trioxide. Arkiv foer Kemi, 21, 357–364.
Le Bail, A., Duroy, H., and Fourquet, J.L. (1988) Ab initio structure determination of $LiSbWO_6$ by X-ray powder diffraction. Materials Research Bulletin, 23, 447–452.
Libowitzky, E. (1999) Correlation of O-H stretching frequencies and O-H···O hydrogen bond lengths in minerals. Monatshefte für Chemie, 130, 1047–1059.
Liss, K.-D., Hunter, B.A., Hagen, M.E., Noakes, T.J., and Kennedy, S.J. (2006) Echidna—the new high-resolution powder diffractometer being built at OPAL. Physica B, 385–386, 1010–1012.
Matsubara, S., Kato, A., and Nagashima, K. (1984) Mpororoite and anthoinite from the Kara mine, Tasmania. Mineralogical Magazine, 48, 397–400.
Niggli, E. and Jager, E. (1957) Untersuchungen an anthoinit. Neues Jahrbuch für Mineralogie, Abhandlungen, 91, 35–40.
Rodriguez-Carvajal, J. (1990) FULLPROF: A program for Rietveld refinement and pattern matching analysis. Satellite meeting on powder diffraction of the XV Congres of the IUCr, Toulouse, France.
Sahama, T.G. (1981) The secondary tungsten minerals, a review. The Mineralogical Record, March-April, 81–87.
Sahama, T.G., Von Knorring, O., and Lehtinen, M. (1970) New data for anthoinite. Bulletin of the Geological Society of Finland, 42, 95–99.
Skarstad, P.M. and Geller, S. (1975) $(W_4O_{16})^{8-}$ polyion in the high temperature modification of silver tungstate. Materials Research Bulletin, 10, 791–800.
Varlamoff, N. (1947) Anthoinite, nouveau tungstate hydrate d'alumine. Annales de la Société géologique de Belgique, 70, B153–B156.
Von Knorring, O., Sahama, T.G., and Lehtinen, M. (1972) Mpororoite, a new secondary tungsten mineral from Uganda. Bulletin of the Geological Society of Finland, 44, 107–110.

Manuscript received August 20, 2009
Manuscript accepted November 17, 2009
Manuscript handled by Ian Swainson